Cement and Concrete Research 38 (2008) 1049–1060

Contents lists available at ScienceDirect

Cement and Concrete Research

journal homepage: http://ees.elsevier.com/CEMCON/default.asp

# Effect of specimen size on fracture energy and softening curve of concrete: Part I. Experiments and fracture energy

Zhifang Zhao [a], Seung Hee Kwon [b,*], Surendra P. Shah [c]

[a] College of Civil Engineering and Architecture, Zhejiang University of Technology, Hangzhou, Zhejiang 310014, PR China
[b] Department of Civil and Environmental Engineering, Myongji University, San 38-2 Namdong, Cheoingu, Yongin, Gyeonggi-do, 449-728, Republic of Korea
[c] Center for Advanced Cement-Based Materials, Northwestern University, 2145 Sheridan Road, A130, Evanston, IL, 60208, USA

ARTICLE INFO

*Article history:*
Received 22 October 2007
Accepted 18 March 2008

*Keywords:*
Fracture energy
Three-point bend test
Wedge splitting test
Size effect

ABSTRACT

The fracture energy of concrete $G_F$ is a fundamental fracture parameter, presenting the concrete's cracking resistance. However, because of the experimentally observed size dependency, it remains controversial as to whether the fracture energy can be considered as a material property. In this study, a three-point bend test for a notched beam and a wedge splitting test were performed with different size specimens for ten different concrete mixes in order to investigate the effect of specimen size and geometry on the fracture energy. A data processing method was proposed for averaging the test results of companion specimens, and the fracture energy was calculated from the averaged results. From a comparison of the fracture energies, it was found that the fracture energy increases with an increase in specimen size in both the beam and wedge splitting tests.

© 2008 Elsevier Ltd. All rights reserved.

## 1. Introduction

Fracture energy is a fundamental fracture parameter, representing cracking resistance and fracture toughness of concrete, and is generally considered as a material property in concrete fracture mechanics and cracking analyses. However, it remains controversial as to whether or not the fracture energy is size dependent. Existing studies [1–5] have shown that the experimentally determined fracture energy increases with increased specimen size. Some researchers have argued that the fracture energy is a material property, and the observed size effect is caused by several sources of experimental error, the testing procedure or limitations of the three-point bend test in finding the fracture energy [6–10]. In practice, three-point bend tests are performed in most studies on size effect of fracture energy; however, this testing method could entail considerable experimental error, as noted in the literature [7–9]. Hu and Wittmann [11] here stated that the size effect is caused by variation in the width of the fracture process zone according to the ligament length of the specimen.

In order to more clearly verify the effect of specimen size and geometry on the fracture energy, three-point bend tests for a notched beam and wedge splitting tests were performed simultaneously for thirty-four specimens comprised of ten different concrete mixes, where the maximum size of coarse aggregate and the water to binder ratio were varied. The load-deflection and the load-CMOD measured from the companion specimens were averaged by a data processing method suggested in this study, and the fracture energy for each specimen was calculated from the averaged data. From the calculated fracture energy for every specimen, the effects of specimen size, geometry, aggregate size, and water to binder ratio on the fracture energy are analyzed and discussed.

## 2. Experiments

### 2.1. Materials

Table 1 shows the concrete mix proportions. There are three groups of concrete mixes; SG group is concrete made of small size gravel, LG group is dam concrete, and WG group is wet-screening concrete where the gravel of more than 40 mm is removed through screening the fresh mixes, LG1 and LG2, respectively. Type IV cement, fly ash, crushed gravel, and river sand were used in all the mixes. The water to binder ratio was ranged from 0.30 to 0.50, and the gravel size from 10 mm to 80 mm. The substitution rate of fly ash was 10–30% for the total binder content.

### 2.2. Test program

Table 2 shows the test program. Both three-point bend tests for a notched beam and wedge splitting tests were performed for the six

* Corresponding author.
*E-mail address:* kwon08@mju.ac.kr (S.H. Kwon).

0008-8846/$ – see front matter © 2008 Elsevier Ltd. All rights reserved.
doi:10.1016/j.cemconres.2008.03.017

**Table 1**
Mix proportions

| Concrete mix | | w/b | Maximum gravel size | Unit weight(kg/m$^3$) | | | | | | |
|---|---|---|---|---|---|---|---|---|---|---|
| | | | | c | w | F.A | S | G | W.R. | A.E. |
| SG | 1 | 0.50 | 10 mm(0.4 in.) | 196 | 140 | 84 | 869 | 1090 | 1.68 | 0.0196 |
| | 2 | 0.50 | 20 mm(0.8 in.) | 185 | 132 | 79 | 846 | 1152 | 1.58 | 0.0185 |
| | 3 | 0.45 | 20 mm(0.8 in.) | 240 | 135 | 60 | 814 | 1154 | 1.80 | 0.0195 |
| | 4 | 0.35 | 20 mm(0.8 in.) | 309 | 135 | 77 | 744 | 1145 | 2.32 | 0.0251 |
| | 5 | 0.30 | 20 mm(0.8 in.) | 420 | 140 | 47 | 698 | 1121 | 2.80 | 0.0280 |
| | 6 | 0.50 | 40 mm(1.6 in.) | 168 | 120 | 72 | 769 | 1287 | 1.44 | 0.0168 |
| LG | 1 | 0.45 | 80 mm(3.1 in.) | 159 | 102 | 68 | 625 | 1496 | 1.36 | 0.0159 |
| | 2 | 0.50 | 80 mm(3.1 in.) | 143 | 102 | 61 | 653 | 1491 | 1.22 | 0.0143 |
| WG | 1 | 0.45 | 40 mm(1.5 in.) | 159 | 102 | 68 | 625 | 1496 | 1.36 | 0.0159 |
| | 2 | 0.50 | 40 mm(1.5 in.) | 143 | 102 | 61 | 653 | 1491 | 1.22 | 0.0143 |

SG; small gravel concrete, LG; large gravel concrete, WG; wet-screening concrete.

mixes, SG1 to SG6. The beam tests were carried out for LG1 and WG1, and the wedge splitting tests for LG2 and WG2. The mixes SG1, SG2, LG1, LG2, WG1, and WG2 have from two to five different size specimens for the beam and wedge splitting tests. The tests were designed so as to allow for comparison of the test results according to the specimen size, maximum aggregate size, water to binder ratio, and testing method for ten different concrete mixes.

### 2.3. Specimen and test set-up

Fig. 1 shows the geometry of the beam and wedge specimens, and the dimensions are listed in Tables 3 and 4. In addition to the fracture tests, tests for compressive strength and secant modulus were performed following the ASTM C 469-94 [12] at an age of 1 year. Compressive strength and elastic modulus were determined based on an averaged result of three identical 150×150×150 mm cubes and $\Phi$150×300 mm cylinders, respectively. The mold for each specimen was removed 1 day after casting, and each specimen was cured by spraying water on the surface to prevent drying during a period of 28 days. All the mixes were designed for an actual dam built in China, and the specimens were kept in the same environmental condition as the dam for 1 year after curing. The characterization specimens were also stored together with the fracture specimens.

Every test was performed at the age of 1 year. Four companion specimens were manufactured for each test variable, but some specimens were broken in handling and moving and reliable test results could not be obtained for some specimens. The numbers of companion specimens that were employed in the beam and wedge splitting tests and provided reliable data are also listed in Tables 3 and 4.

Fig. 2(a) shows the set-up for the three-point bend beam test. The tests were conducted in a very stiff servo-hydraulic closed-loop testing machine. A 100 kN capacity load cell was used to measure the applied load, and the accuracy was ±2% of the maximum applied load. The crack mouth opening displacement (CMOD) was measured with a displacement sensor having a capacity and accuracy of 5 mm and ±0.0005 mm, respectively. The vertical deflection was also measured at the loading point. The loading actuator was controlled by a constant CMOD rate of 0.15 mm/min.

Some wedge splitting specimens were much larger than ordinary size, because large size coarse aggregate was used. One line support is generally located in the center of the wedge specimen [13–15]. In contrast with an ordinary wedge splitting test, two line supports located in the center of the half section of the specimen were used in order to circumvent difficulties in handling the very large size specimen and to prevent unexpected failure of the specimen while preparing the test. As shown in Fig. 2(b), two massive steel loading devices equipped with roller bearings on each side were placed on top of the specimen. A steel profile with two identical wedges was fixed at the upper plate of the testing machine. The wedges enter between the bearings, which apply a horizontal splitting force ($P_S$). The displacement sensor and load cell were identical to those used in the beam test. The axis of the roller was aligned with the displacement sensor, that is, the displacement was measured at the horizontal loading axis. The wedge splitting test was also controlled by a constant CMOD rate of 0.15 mm/min. Fig. 3 shows the real test set-up.

To make the notch in every specimen, steel plate with the thickness of 2 mm was fixed in the molds before casting, and the surfaces facing concrete were painted with lubricating oil to prevent friction between the plate and concrete. When demolding, the steel plate was carefully removed.

## 3. Data processing for companion specimens

### 3.1. Averaging the data for companion specimens

There were two to four companion specimens for each test. In order to find the fracture characteristics for each test, it is necessary to average the test results for the companions. However, the averaged results may depend on the method used to average the data. The method used to process the test results for the companion specimens is described below.

In Fig. 4, the data processing procedure for three companion specimens of LG2-W1 is illustrated as an example for beam and wedge splitting specimens. Fig. 4(a) shows the raw test data for three companion specimens, where the total number of raw data for each specimen was about 50,000. The data scattered far from the load-CMOD curve are first filtered and then one point is taken every 20 points in the load-CMOD curve. Around a given point, an average was taken of five points consisting of the given point, and two points above and below the given point. By averaging the five adjacent points, the effect of fluctuation in the measurement can be removed. Fig. 4(b) shows the results after filtering and averaging for each companion. The peak load point of each specimen are taken from the results given

**Table 2**
Test program

| Concrete mixes | Test method | |
|---|---|---|
| | Beam | Wedge |
| SG1 | ○ | ○ |
| SG2 | ○ | ○ |
| SG3 | ○ | ○ |
| SG4 | ○ | ○ |
| SG5 | ○ | ○ |
| SG6 | ○ | ○ |
| LG1 | ○ | X |
| LG2 | X | ○ |
| WG1 | ○ | X |
| WG2 | X | ○ |

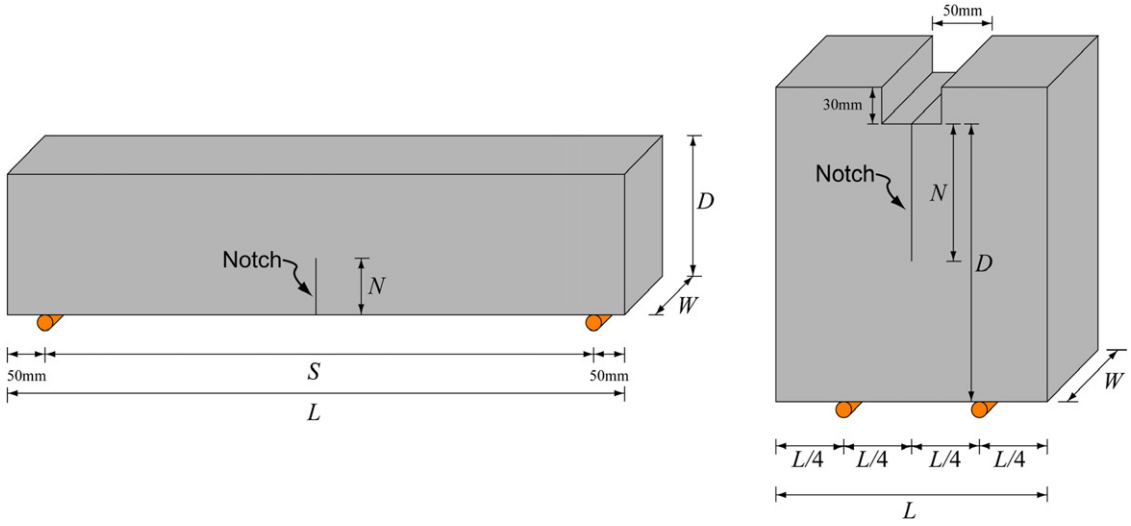


**Fig. 1.** Geometry of notched beam and wedge splitting specimens.

in Fig. 4(b), and then 100 equally spaced CMOD values are calculated from the zero point to the CMOD at the peak point and from the peak to the end point, respectively. The end point of CMOD for each specimen is set such that the distance from the peak to the end point is identical for each three specimens, for example, 3.8 mm from the CMOD at the peak in the case of the LG2-W1 specimen. The load

**Table 3**
Dimensions of beam specimens

| Concrete mix | Specimen | Number of companion specimens | Dimensions of beam specimen | | | |
|---|---|---|---|---|---|---|
| | | | *D* (mm) | *L*/*S* (mm) | *N* (mm) | *W* (mm) |
| SG1 | B1 | 3 | 300 | 1300/1200 | 120 | 120 |
| | B2 | 2 | 400 | 1700/1600 | 160 | |
| SG2 | B1 | 3 | 150 | 700/600 | 60 | |
| | B2 | 2 | 200 | 900/800 | 80 | |
| | B3 | 3 | 300 | 1300/1200 | 120 | |
| | B4 | 2 | 400 | 1700/1600 | 160 | |
| | B5 | 2 | 500 | 2100/2000 | 200 | |
| SG3 | B1 | 3 | 300 | 1300/1200 | 120 | |
| SG4 | B1 | 3 | 300 | 1300/1200 | 120 | |
| SG5 | B1 | 3 | 300 | 1300/1200 | 120 | |
| SG6 | B1 | 3 | 300 | 1300/1200 | 120 | |
| LG1 | B1 | 2 | 400 | 1700/1600 | 160 | 240 |
| | B2 | 2 | 450 | 1900/1800 | 180 | |
| | B3 | 4 | 500 | 2100/2000 | 200 | |
| | B4 | 3 | 550 | 2300/2200 | 220 | |
| WG1 | B1 | 2 | 250 | 1100/1000 | 100 | 120 |
| | B2 | 3 | 300 | 1300/1200 | 120 | |
| | B3 | 3 | 400 | 1700/1600 | 160 | |

**Table 4**
Dimensions of wedge splitting specimens

| Concrete mix | Specimen | Number of companion specimens | Dimensions of wedge splitting specimen | | | |
|---|---|---|---|---|---|---|
| | | | *D* (mm) | *L* (mm) | *N* (mm) | *W* (mm) |
| SG1 | W1 | 3 | 300 | 300 | 150 | 200 |
| | W2 | 2 | 600 | 600 | 300 | |
| SG2 | W1 | 2 | 300 | 300 | 150 | |
| | W2 | 3 | 600 | 600 | 300 | |
| | W3 | 3 | 800 | 800 | 400 | |
| | W4 | 3 | 1000 | 1000 | 500 | |
| SG3 | W1 | 3 | 300 | 300 | 150 | |
| SG4 | W1 | 2 | 300 | 300 | 150 | |
| SG5 | W1 | 3 | 300 | 300 | 150 | |
| SG6 | W1 | 3 | 300 | 300 | 150 | |
| LG2 | W1 | 3 | 450 | 450 | 225 | 250 |
| | W2 | 2 | 800 | 800 | 400 | |
| | W3 | 3 | 1000 | 1000 | 500 | |
| WG2 | W1 | 2 | 300 | 300 | 150 | 200 |
| | W2 | 2 | 600 | 600 | 300 | |
| | W3 | 3 | 800 | 800 | 400 | |

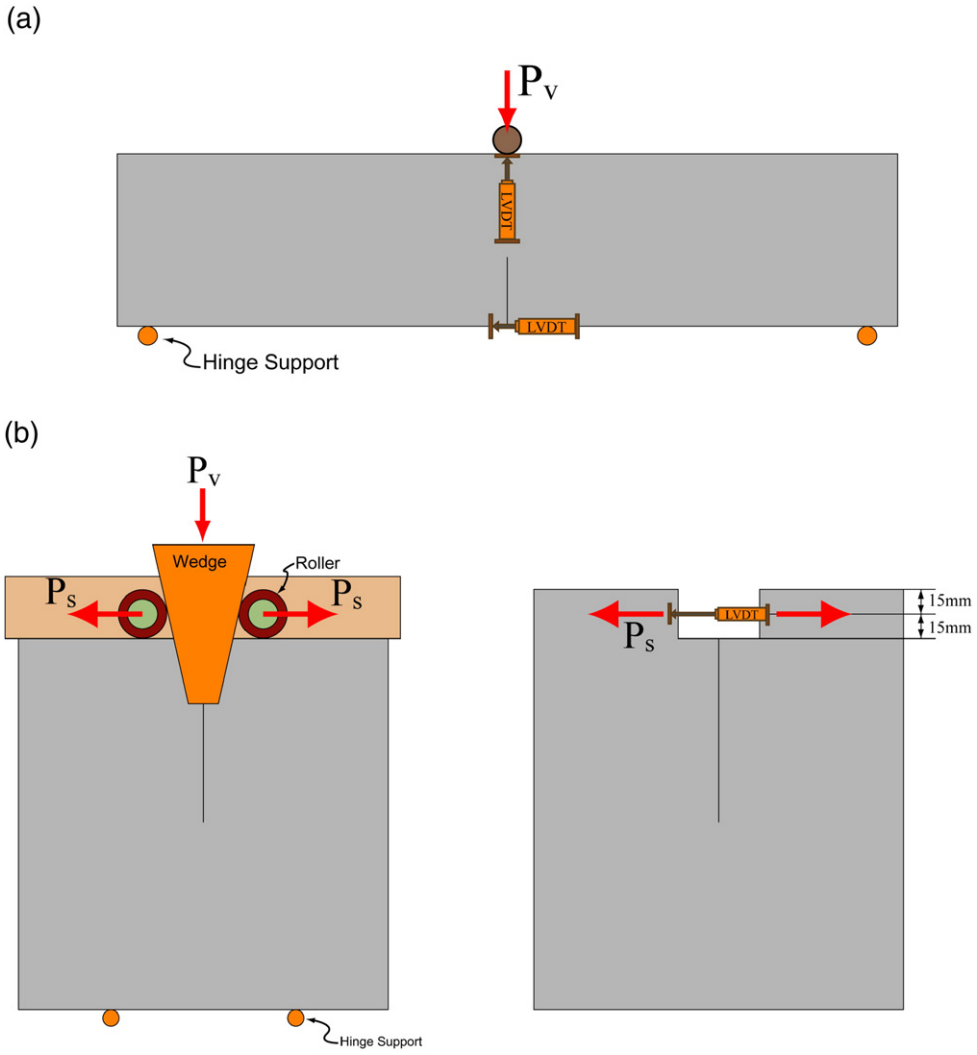


**Fig. 2.** Configuration of test set-ups. (a) Three-point bend beam test. (b) Wedge splitting test.

values corresponding to the 100 CMOD values are calculated by interpolation between the averaged data points of Fig. 4(b) for ascending and descending parts. Now, we have two hundreds data points, one hundred each for ascending and descending parts. The three ascending curves for each of the three specimens(LG2-W1-1, LG2-W1-2 and LG2-W1-3) are shown in Fig. 4(c) and (d).

According to the equivalent elastic crack approach based on the Griffith–Irwin cracking mechanism [16–18], the fracture process zone (FPZ) is formed with an increase of the applied load, and the equivalent extension of the crack length, which is elastically equivalent to the process zone, is largest at the peak. After the peak load, the process zone starts to move forward along the crack path, maintaining the largest equivalent extension size c, as shown in Fig. 5. When averaging the test data between the companions, each averaging point of the data has to represent the same fracture status. The 100th data point represents the peak load status for each specimen, and is in the same fracture status. For each of the equally spaced 100 CMODs up to the peak and the corresponding loads, the *i*th data point for each specimen can be assumed to be in the same status, namely, the *i*th step of increasing the fracture process zone. The end points (200th data points) of the descending part in Fig. 4(d) represent the same status that the largest equivalent extension is moved the same distance from the peak point. The *i*th data point in the descending region can also be considered as the same status that the fracture process zone is equally far from the peak, because each data point is equally spaced. Therefore, 200 equally spaced CMOD values and the corresponding load values for each specimen can be averaged. The averaged load-CMOD curve is shown in Fig. 4(e).

### *3.2. Extracting the data points representing the load-CMOD curve*

The data sets are prepared for an inverse analysis to find the softening curve, which will be presented in Part II. Because the number of data points used in optimal fitting significantly affects the computer running time, the minimum number of data points sufficiently representing the load-CMOD curve is desirable. From the averaged data for the companion specimens, the minimum data points were extracted using an optimization technique.

A multi-linear function was employed to fit the ascending part of Fig. 4(f). The points comprising the multi-linear lines were assumed to be on the line interpolated between the averaged data points. Several multi-linear functions were tried, and it was found that the multi-linear function consisting of seven lines accurately fit the ascending part. With more than seven lines, the accuracy was almost identical. The Marquardt–Levenberg method [19] was used in the optimization, and the coefficient of determination was more than 0.99 for all cases. Six points excluding the origin and the peak point were found for the ascending part of every beam and wedge splitting specimen.

(a)

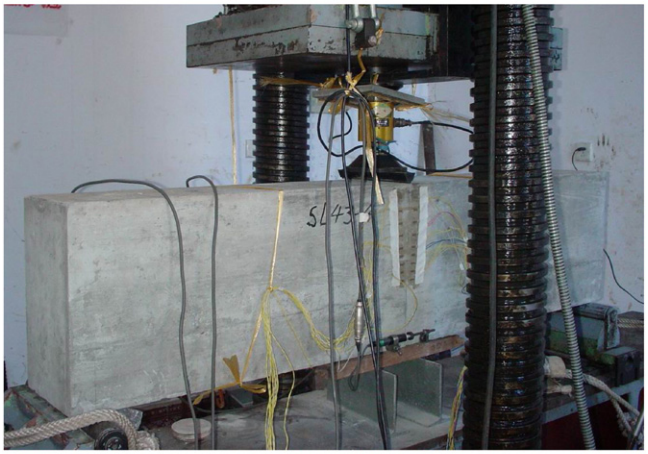

(b)


**Fig. 3.** Real test set-ups. (a) Three-point bend beam test. (b) Wedge splitting test.

For the descending part, the data points equally spaced over the CMOD axis were extracted. Minimum twelve points were needed for an accurate fit. Twelve points excluding the peak and the end point points were selected, and the coefficient of determination for the multi-linear function consisting of the selected points was more than 0.99. A total of twenty points including the peak and the end point were extracted from the averaged load-CMOD curve, as shown in Fig. 4(f).

## 4. Test results and discussion

Table 5 shows the compressive strength, the secant modulus, and the tangent modulus at 1 year age for every concrete mix. Because the inelastic strain is included when calculating the secant modulus, the initial tangent modulus excluding the inelastic part was calculated by the following equation of the CEB-FIP model code [20], which will also be used in the inverse analysis of Part II.

$$E_{ci} = E_c/0.85 \tag{1}$$

In the equation, $E_c$ and $E_{ci}$ are the secant and tangent modulus, respectively. The averaged load-deflection curves for the beam specimens are shown in Fig. 6. Figs. 7 and 8 show the load-CMOD curve consisting of 20 data points(7 points for ascending and 13 points for descending) corresponding to Fig. 4(f) for every beam and wedge specimen.

Peak loads measured from the beam and wedge splitting specimens are compared in Fig. 9. The peak loads of the beam and wedge specimens, SG1, SG2, LG1, WG1, LG2 and WG2, increase with increasing the specimen size, as shown in Fig. 9(a) and (b). For the same size beam specimens, SG1-B1, and SG3-B1 to SG6-B1, the peak loads of SG1 and SG5 are the lowest and the largest, respectively. Similarly, for the same size wedge specimens, SG1-W1, SG2-W1, and SG3-W1 to SG6-W1, the peak loads of SG1 and SG5 are also the lowest and the largest, respectively. This appears to be attributable to the effect of the water–binder ratio.

The fracture energy for each specimen was calculated from the test results and is compared according to size in Figs. 10–12. In the case of the beam specimen, the fracture energy was calculated based on the following equation of Rilem recommendation [21], and the self weight effect was also considered.

$$G_F = \frac{W_1 + mg\delta_0}{(D-N)W} \tag{2}$$

In Eq. (2), $G_F$ is the fracture energy, $W_1$ is the area under the load-deflection curve of Fig. 6, $m$ is the total mass of the specimen, $g$ is gravity, $\delta_0$ is the end deflection at $P$=0, and $D$, $N$, and $W$ are the depth, notch length, and width of the specimen, respectively. The fracture energy for the wedge *specimen* was calculated from the load-CMOD of Fig. 7 using the following equation; note that the self weight of the wedge specimens was not considered, because the self weight is borne by the two bottom supports, as shown in Fig. 2(b), and is balanced to the reaction at the supports.

$$G_F = \frac{W_1}{(D-N)W}, \quad P_s = \frac{P_v}{2\tan\theta} \tag{3}$$

In Eq. (3), $W_1$ is the total work of the area under the load-CMOD curve of Fig. 8, $P_s$ is the horizontal load, $P_v$ is the applied vertical load, and $\theta$ is the wedge angle, which was 15° in the test set-up. The tests did not proceed until a full tail of the load-deflection curve and the load-CMOD curve, respectively, was obtained, and the tail part that is not measured was assumed to be a straight line with the last slope of the load-deflection and load-CMOD curves in the calculation of fracture energy.

The fracture energy calculated from the different size beam specimens is plotted over their depth in Fig. 10(a). It is seen that the fracture energy increases slightly with size in SG1, SG2, and WG1 concrete, and there is no increasing tendency with size in LG1. The difference between the maximum and the minimum fracture energies was 20–30% of the maximum value.

The sources of error in the calculation of the fracture energy from the beam test have previously been investigated by Guinea et al. [7], Planas et al. [8], and Elices et al. [9]. The main sources were the friction between the support and the specimen, crushing near the supports, the energy dissipation in the bulk of the materials near the crack, and the energy enclosed in the unmeasured tail part of the load-deflection curve. It was found in these studies that the observed size dependence of the fracture energy of about 40% was caused by these sources, and the size-independent fracture energy could be obtained from correction of these errors. The majority of the error, more than 30% of the observed size dependence of 40%, originated from the neglected energy of the tail part. When these sources of error are considered in the calculation of the fracture energy for the beam tests of this study, it is not clear whether the 20–30% size dependence of Fig. 10(a) is an intrinsic feature of concrete material or is caused by inevitable test error.

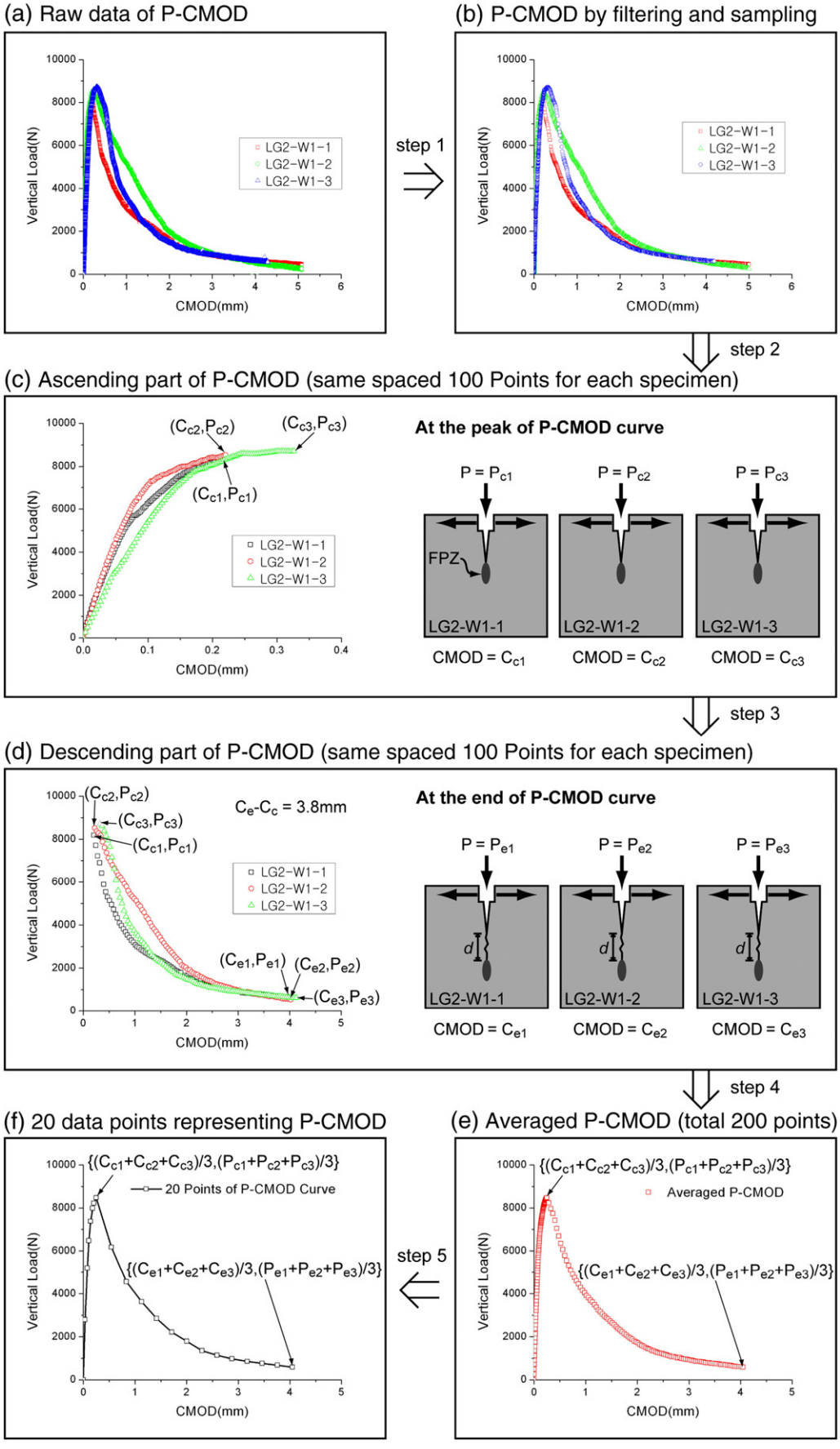


**Fig. 4.** Data processing for beam and wedge splitting specimens.

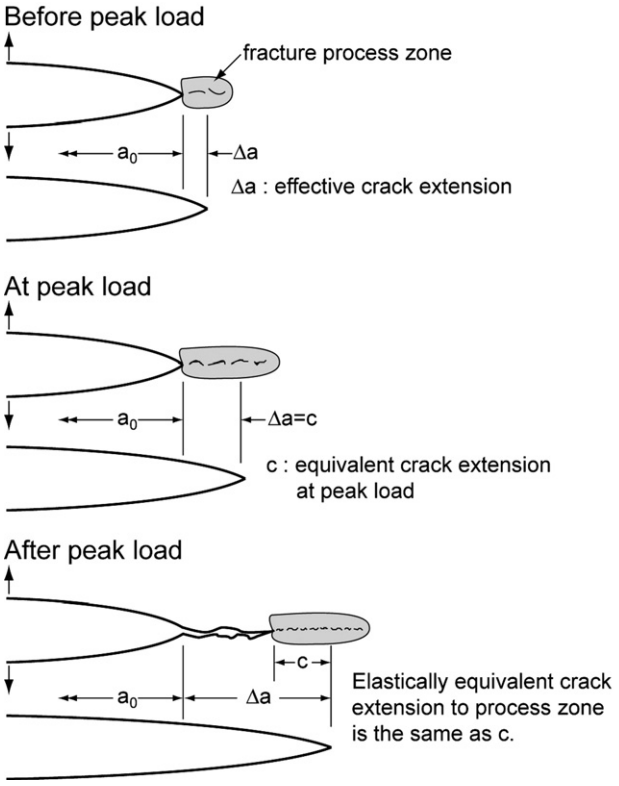


**Fig. 5.** Fracture process zone and equivalent crack extension at different fracture stages [18].

Unlike in the beam tests, some experimental error can be avoided in the wedge splitting tests. Because the vertical load is not applied to the specimen and only lateral force acts by the wedge and roller, the energy dissipation not related to crack propagation such as friction of the support and crushing near the support can be minimized. The self weight was also compensated in the test set-up by using two bottom supports. Therefore, if the size dependence observed in the beam tests is due to an artefact, there would be no or less size dependence in the fracture energy obtained from the wedge splitting tests for the same concrete. As shown in Fig. 10(b), however, the fracture energy obtained from the wedge specimens also increases over size, and the difference between the maximum and the minimum fracture energies was 30–60% of the maximum value (140%–250% of the minimum value). It is seen that the size dependence in the wedge splitting tests is much larger than that in the beam tests. Even if the sources noted above are considered, it is difficult to explain this amount of size dependence. Therefore, it can be concluded that the fracture energy of concrete depends on the specimen size.

In a previous study by Wittmann et al. [2], wedge splitting tests were performed with three different size specimens, and the size effect of the fracture energy, i.e., a maximum of 30% fracture energy difference for one to four times size specimens, has been observed. They also attempted to find the softening curve by optimally fitting the test results using an optimization technique, and the influence of the size dependent fracture energy on the softening curve was analyzed. However, this study was conducted only for one concrete and thus more extensive investigation of the size effect of the softening curve is needed (this will be carried out by the present authors in our subsequent paper).

The size effect of fracture energy can be explained in terms of variation of the influence of the fracture process zone on fracturing according to the size and geometry of the specimen. This is because the whole body except the process zone can be assumed to be elastic in the beam and wedge splitting tests, although some regions near the support and the loading point are in an inelastic state, but do not contribute to cracking. Hu and Wittmann [11] introduced a local fracture energy concept where the fracture energy varies with the width of the process zone. They explained the size dependent fracture energy in terms of different distributions of the local fracture energy according to the shape of the process zone, which depends on the size and geometry of the specimen. However, the mechanism of the process zone is still not fully understood.

The fracture energy of SG2 and LG2 increases up to the second largest size and drops slightly at the largest size, as shown in Fig. 10(a) and (b). It appears that the fracture energy does not decrease but rather it approaches a certain value with an increase of the size. This asymptotic behaviour was also observed in Wittmann, Mihashi and Nomura's experimental work [2]. Further study on the mechanism of the process zone inducing the increase of fracture energy and the asymptotic feature is needed.

The beam and wedge splitting tests were performed for ten different concretes, and the fracture energies were analyzed according to the maximum aggregate size and the water to binder ratio, as presented in Fig. 11, where $d_a$ is the maximum aggregate size. Because of the possible size effect, the fracture energies for the same size specimens were compared. In Fig. 11(a), the effect of the gravel size does not clearly appear in the beam tests, but the wedge test results distinctly show the effect. As noted above, the beam test results may include more experimental error compared to the wedge splitting test, which seems to hinder the effect on the gravel size in the beam tests. The fracture energies of WG2-W3 and LG2-W2 are much higher than others. In these cases, the specimen sizes (800 mm depth) are more than double those of the other specimens. The effect of gravel size on fracture energy found in this study is in accordance with the findings of the literature [22]. As shown in Fig. 11(b), there is no increasing or decreasing trend in the fracture energy for the water to binder ratio. The values given at the bottom of the bar are the measured compressive strength and the fracture energy is for the same depth of 300 m, as presented in Fig. 11(b). Generally, the fracture energy increases with an increase of the compressive strength, which strongly depends on the water to binder ratio. However, the substitution ratio of fly ash to the cement was different in each mix. There was little difference in the strength in SG3 to SG5, although the water to binder ratio varied from 30 to 45%. Therefore, the water to binder ratio apparently cannot be directly correlated to the fracture energy in this study.

The fracture energies obtained from the beam and wedge splitting tests for SG1 to SG6 concrete are compared in Fig. 12. Because the possible energy dissipation in regions other than the fracture process zone, the experimentally determined fracture energy from the beam test is expected to be larger than that of the

**Table 5**
Mechanical properties

| Concrete mix | Compressive strength (MPa) | Secant modulus (GPa) | Initial tangent modulus (GPa) |
|---|---|---|---|
| SG1 | 43.8 | 26.7 | 31.4 |
| SG2 | 43.4 | 33.3 | 39.2 |
| SG3 | 50.9 | 30.4 | 35.7 |
| SG4 | 56.4 | 30.5 | 35.9 |
| SG5 | 50.2 | 34.8 | 41.0 |
| SG6 | 50.8 | 33.1 | 38.9 |
| LG1 | 40.0 | 28.6 | 33.6 |
| LG2 | 51.7 | 33.7 | 39.6 |
| WG1 | 40.0 | 28.6 | 33.6 |
| WG2 | 51.7 | 33.7 | 39.6 |

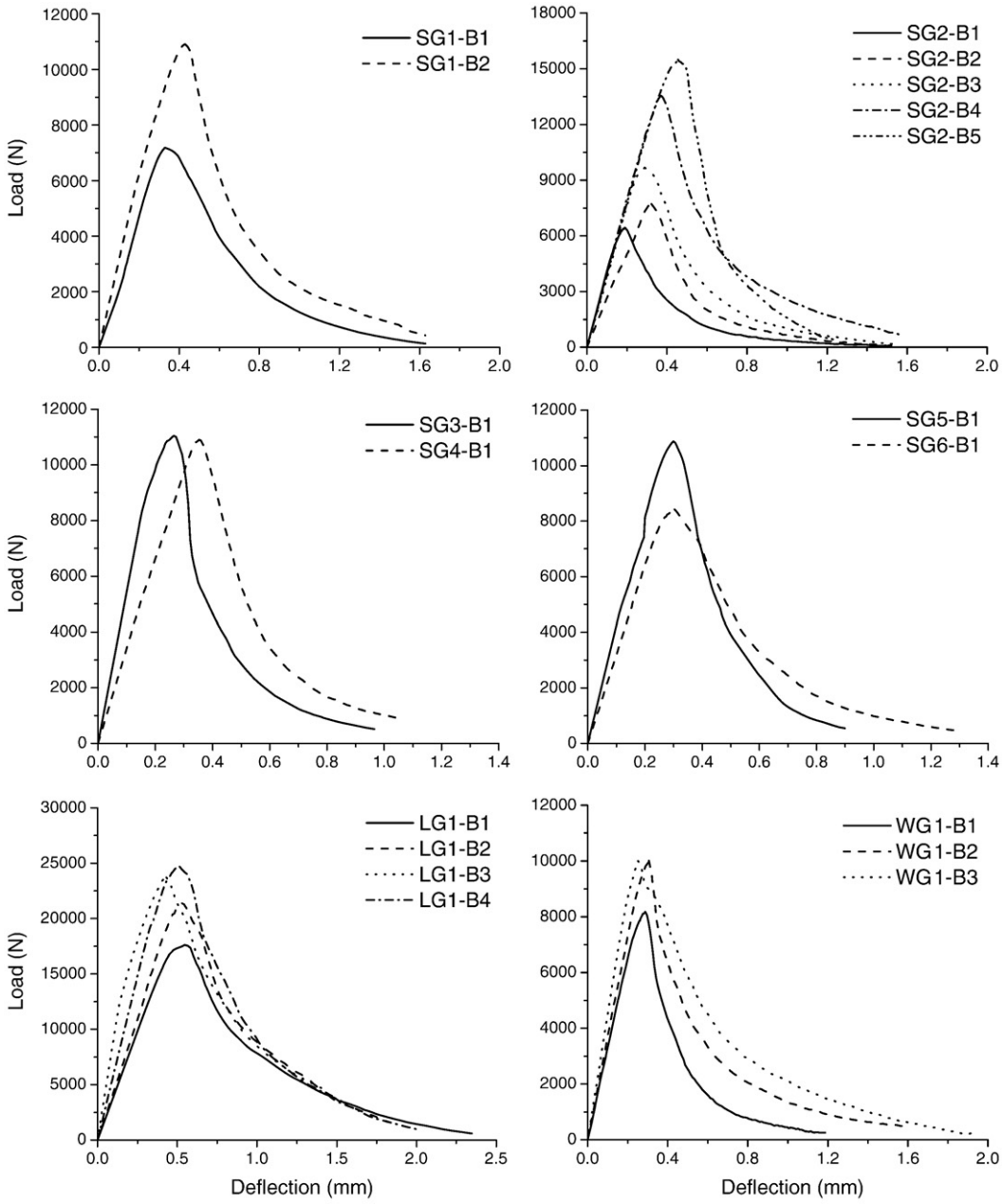


**Fig. 6.** Load-deflection curves for beam specimens.

wedge test. However, there is no systematic trend between the beam and wedge geometry. Because of the different stress and strain distribution according to the geometry, the shape of the process zone might be affected by the geometry of the specimen as well as the aggregate size and the mix proportion of the matrix [17]. In order to explain the difference of the fracture energies obtained from the two tests, every influencing factor on the process zone, including the specimen size and geometry, the aggregate size, and the mechanical properties of the matrix, should be considered.

A qualitative analysis was performed for the experimentally determined fracture energy. In the subsequent paper, the size effect of the fracture energy will be quantitatively examined based on the softening curves obtained from an inverse analysis, and a possible mechanism of the process zone related to the identified features for the fracture energy will be discussed.

## 5. Conclusions

Three-point bend tests for a notched beam and wedge splitting tests were performed for ten different types of concrete with different size specimens. A data averaging method for the companion specimens in the fracture test was proposed, and the fracture energy was calculated from the averaged data for each specimen. From the comparison of the fracture energies, it was found that the fracture energy increases with an increase of the specimen size, especially in the wedge tests, and asymptotic behaviour over the size is observed in some concretes. Additionally, it was shown that the fracture energy increases with an increase of the maximum aggregate size, but there was no systematic trend with the water to binder ratio and the test method. The observed size effect of the fracture energy seems to be attributed to the different shape of fracture process zone according to the specimen size and geometry. Further study is needed to identify the mechanism of the

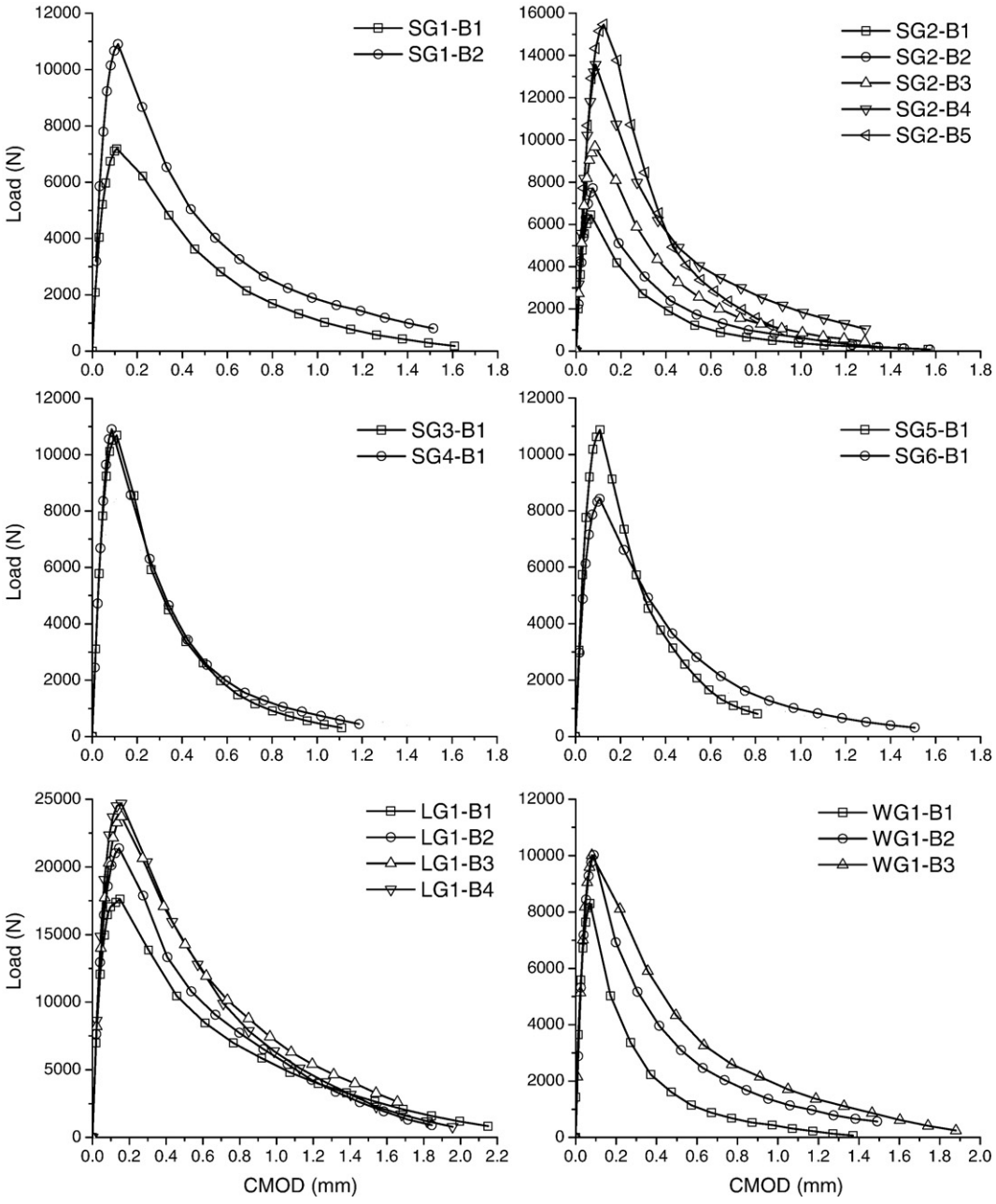


**Fig. 7.** Load-CMOD curves for beam specimens.

process zone. The effect of the size dependent fracture energy on the softening curve will be analyzed from an inverse analysis, and a possible mechanism related to the size effect will be discussed in Part II.

*Notation*

| | |
|---|---|
| CMOD | crack mouth opening displacement |
| $a_o$ | initial crack length |
| $\Delta a$ | effective crack extension |
| $c$ | equivalent crack extension to fracture process zone at the peak |
| $E_c$ | secant modulus of concrete |
| $E_{ci}$ | initial tangent modulus of concrete |
| $G_F$ | fracture energy |
| $W_1$ | total work measured in the beam and wedge splitting tests |
| $m$ | total mass of the beam specimen |
| $g$ | gravity |
| $\delta_0$ | the end deflection at $P=0$ |
| $P$ | applied force |
| $P_v$ | vertically applied force |
| $P_s$ | horizontally applied force |
| $\theta$ | angle of wedge |
| $D$ | depth |
| $N$ | notch length |
| $W$ | width |
| $S$ | span length |
| $L$ | total length of the specimen |
| $d_a$ | maximum aggregate size |
| $f'_c$ | *compressive strength of concrete* |

## Acknowledgments

This work was supported by a grant from Zhejiang Provincial Natural Science Foundation of China (Grant No.Y106486) and National Natural

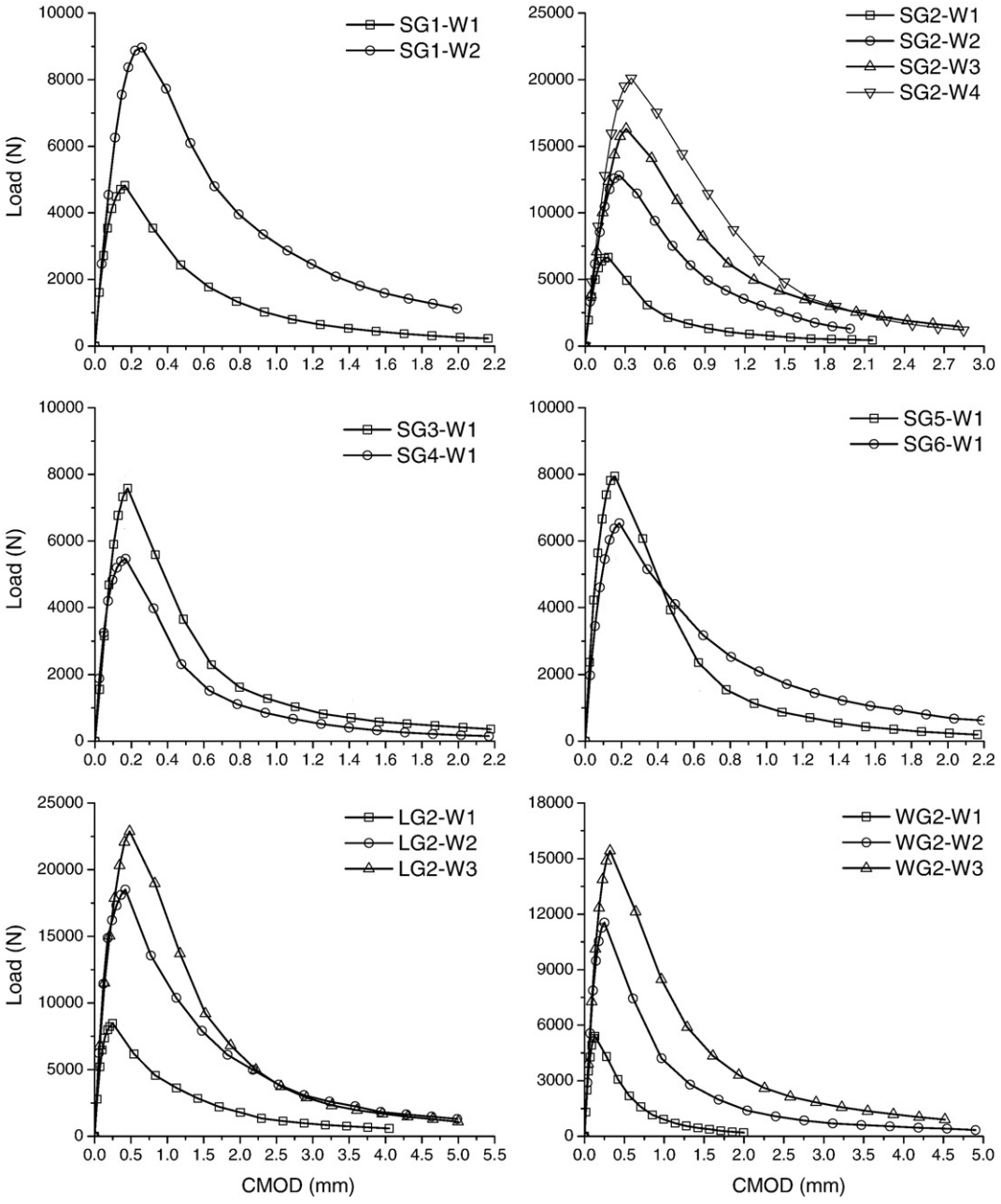


**Fig. 8.** Load-CMOD curves for wedge splitting specimens.

Science Foundation of China (Grant No.50409005). This work was also supported by China Gezhouba (Group) Corporation, Tsinghua University and Yantai University of PR China. They are gratefully appreciated.

This work was also supported by a Korea Research Foundation Grant (KRF-2005-214-D00063).

## References

[1] A. Hillerborg, Results of three comparative test series for determining the fracture energy $G_F$ of concrete, Materials and Structures 18 (107) (1985) 407–413.
[2] F.H. Wittmann, H. Mihashi, N. Nomura, Size effect of fracture energy of concrete, Engineering Fracture Mechanics 35 (1990) 107–115.
[3] .
[4] P. Maturana, J. Planas, M. Elices, Evolution of fracture behavior of saturated concrete in low temperature range, Engineering Fracture Mechanics 35 (1990) 827–834.
[5] S. Xu, G. Zhao, Fracture energy of concrete and its variational trend in size effect studied by using three point bending beams, Journal of Dalian University of Technology 31 (1) (1991) 79–86.
[6] X.H. Guo, R.I. Gilbert, The effect of specimen size on the fracture energy and softening function of concrete, Materials and Structures 33 (2000) 309–316.
[7] G.V. Guinea, J. Planas, M. Elices, Measurement of the fracture energy using three point bend tests: part 1—influence of experimental procedures, Materials and Structures 25 (1992) 212–218.
[8] J. Planas, M. Elices, G.V. Guinea, Measurement of the fracture energy using three point bend tests: part 2-influence of bulk energy dissipation, Materials and Structures 25 (1992) 305–312.
[9] J. Planas, M. Elices, G.V. Guinea, Measurement of the fracture energy using three point bend tests: part 3—influence of cutting the *P–d* tail, Materials and Structures 25 (1992) 327–334.
[10] Q. Jueshi, L. Hui, Size effect on fracture energy of concrete determined by three point bending, Cement and Concrete Research 27 (7) (1997) 1031–1036.
[11] X.Z. Hu, F.H. Wittmann, Fracture energy and fracture process zone, Materials and Structures 25 (1992) 319–326.
[12] ASTM C 469-94, standard test method for static modulus of elasticity and Poisson's ratio of concrete in compression, Annual Book of ASTM Standards, West Conshocken, Pa, 1994.
[13] J.K. Kim, Y. Lee, S.T. Yi, Fracture characteristics of concrete at early ages, Cement and Concrete Research 34 (2004) 507–519.

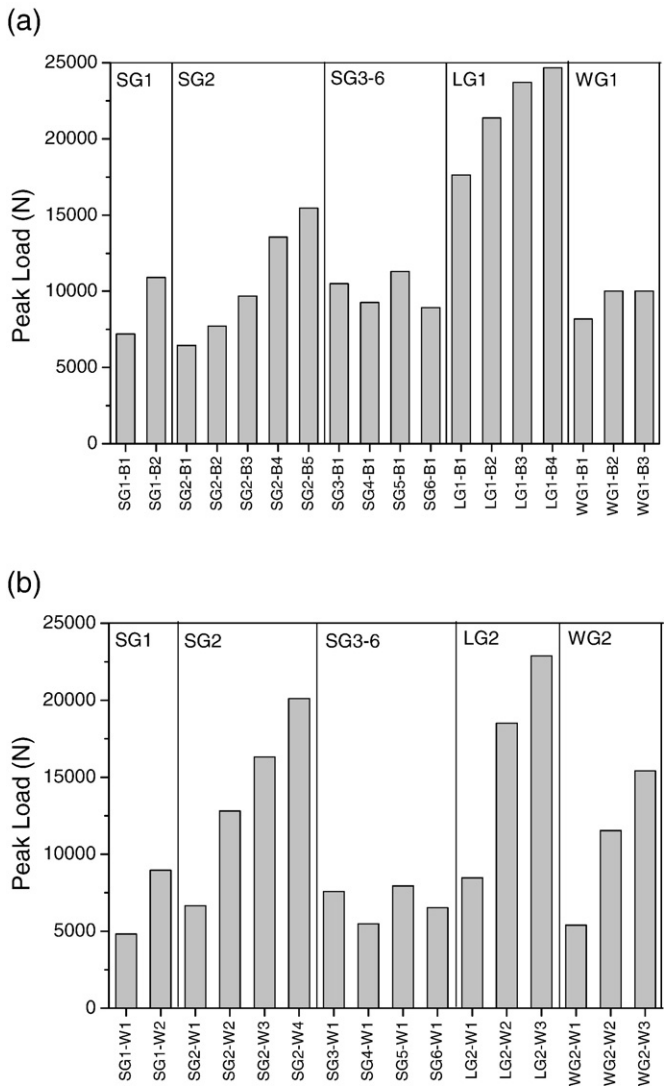


**Fig. 9.** Maximum load. (a) Peak load for beam specimen. (b) Peak load for wedge splitting specimen.

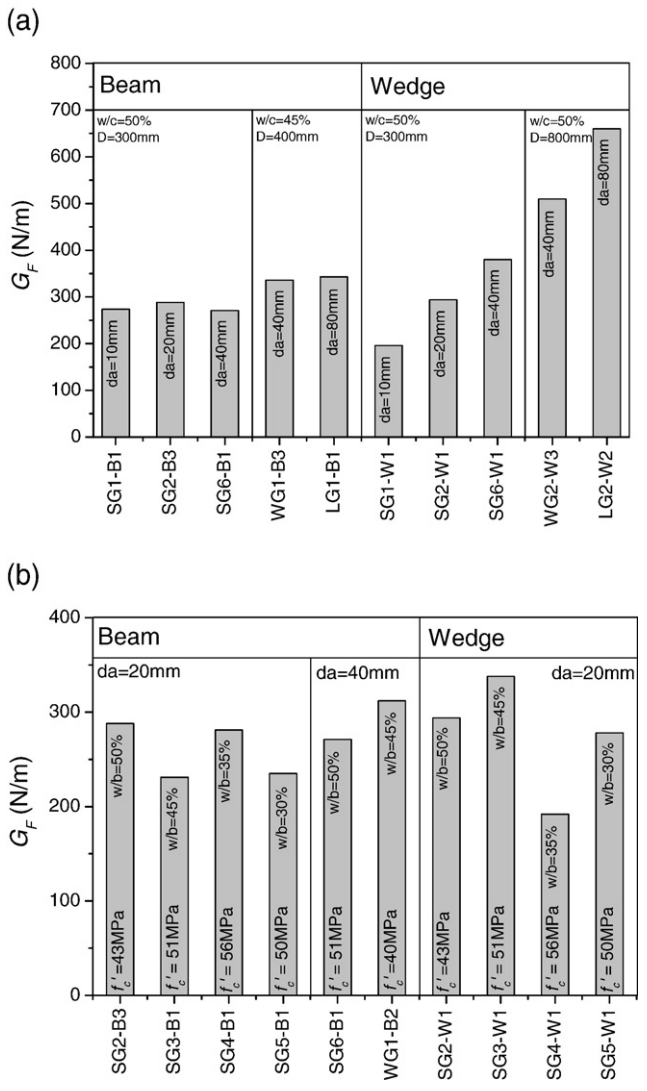


**Fig. 11.** Fracture energy according to gravel size and *w*/*b* ratio. (a) Fracture energy according to maximum gravel size. (b) Fracture energy according to water to binder ratio.

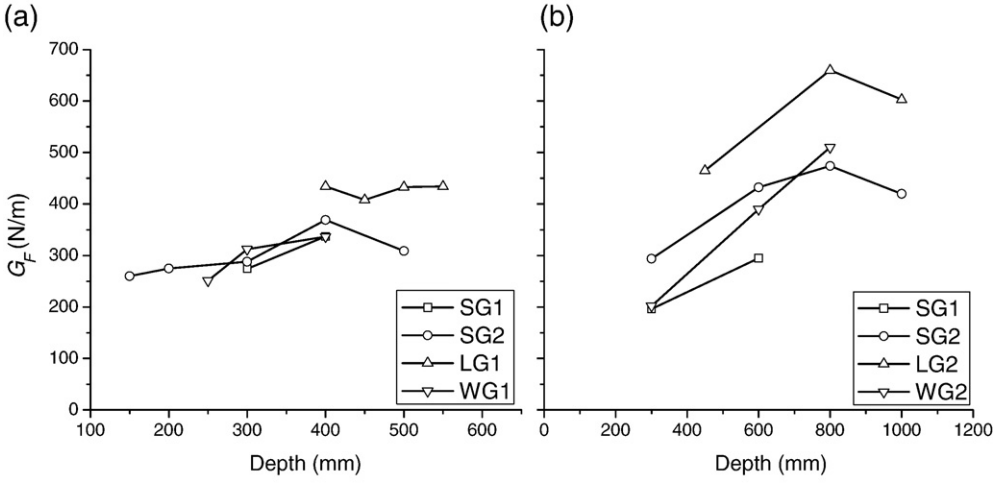


**Fig. 10.** Fracture energy according to specimen size. (a) Beam specimens. (b) Wedge specimens.

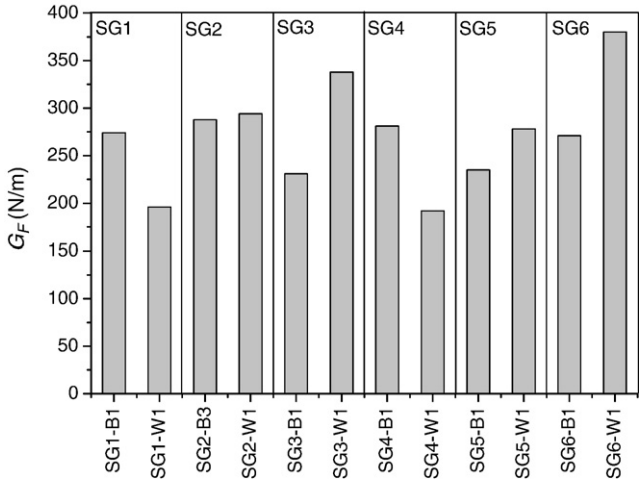


**Fig. 12.** Fracture energy according to Test method.

[14] H.N. Linsbauer, E.K. Tschegg, Fracture energy determination of concrete with cube-shaped specimens, Zement and Beton 31 (1986) 38–40 (in German).
[15] E. Brühwiler, F.H. Wittmann, The wedge splitting test, a new method of performing stable fracture mechanics tests, Engineering Fracture Mechanics 35 (1/2/3) (1990) 117–125.
[16] Y.S. Jenq, S.P. Shah, A two parameter fracture model for concrete, Journal of Engineering Mechanics 111 (4) (1985) 1227–1241.
[17] Z.P. Bazant, M.T. Kazemi, Determination of fracture energy, process zone length and brittleness number from size effect with application to rock and concrete, International Journal of Fracture 44 (1990) 111–131.
[18] Z.P. Bazant, M.T. Kazemi, Size effect in fracture of ceramics and its use to determine fracture energy and effective process zone length, Journal of American Ceramic Society 73 (7) (1990) 1841–1853.
[19] K.M. Brown, Derivative-free analogues of the Levenberg. Marquardt and Gauss algorithms for non-linear least square approximations, IBM, Philadelphia Scientific Center Technical Report, No. 320–2994, 1970.
[20] Comite Euro-International Du Beton, CEB-FIP Model Code 1990, Thomas Telford, 1993.
[21] Rilem TC-50 FMC (Draft Recommendation), Determination of the fracture energy of mortar and concrete by means of three point bend tests on notched beams, Materials and Structures 18 (106) (1985) 285–290.
[22] Szczepan Wolinski, Dirk A. Hordijk, Hans W. Reinhardt, Hans A.W. Cornelissen, Influence of aggregate size on fracture mechanics parameters of concrete, International Journal of Cement Composites and Lightweight Concrete 9 (2) (1987) 95–103.